Synthesis and Structure-Activity Characterization of a Single-Site MoO_2 Catalytic Center Anchored on Reduced Graphene Oxide

Yiqi Liu,[‡1] Jiaqi Li,[‡1] Anusheela Das,[2] Hacksung Kim,[3] Leighton O. Jones,[1] Qing Ma,[4] Michael J. Bedzyk,[*2] George C. Schatz,[*1] Yosi Kratish,[*1] and Tobin J. Marks[*1]

[1]Department of Chemistry and the Institute for Catalysis in Energy Processes (ICEP), Northwestern University, Evanston, Illinois 60208, United States.

[2]Department of Material Science and Engineering and the Institute for Catalysis in Energy Processes (ICEP), Northwestern University, Evanston, Illinois 60208, United States.

[3]Center for Catalysis and Surface Science, Northwestern University, Evanston, Illinois 60208, United States and Chemical Sciences and Engineering Division, Argonne National Laboratory, Lemont, Illinois 60439, United States.

[4]DND-CAT, Northwestern Synchrotron Research Center at the Advanced Photon Source, Argonne National Laboratory, Lemont, Illinois 60439, United States.

KEYWORDS: heterogeneous catalysis, molybdenum, single-site catalysts, carbon supports, structural studies

ABSTRACT: Molecularly-derived single-site heterogeneous catalysts can bridge the understanding and performance gaps between conventional homogeneous and heterogeneous catalysis, guiding the rational design of next-generation catalysts. While impressive advances have been made with well-defined oxide supports, the structural complexity of other supports and the nature of the grafted surface species present an intriguing challenge. In this study, single-site $Mo(=O)_2$ species grafted onto reduced graphene oxide (rGO/MoO_2) are characterized by XPS, DRIFTS, XRD, N_2 physisorption, NH_3-TPD, aqueous contact angle, active site assay poisoning, Mo EXAFS, model compound single-crystal XRD, DFT, and catalytic performance. NH_3-TPD reveals that the anchored MoO_2 moiety is not strongly acidic, while Mo $3d_{5/2}$ XPS assigns the oxidation state as Mo(VI), and XRD shows little rGO periodicity change on MoO_2 grafting. Contact angle analysis shows that MoO_2 grafting consumes rGO surface polar groups, yielding a more hydrophobic surface. The rGO/MoO_2 DRIFTS assigns features at 959 cm^{-1} and 927 cm^{-1}, to the symmetric and *anti*-symmetric Mo=O stretching modes of an isolated *cis*-(O=Mo=O) moiety, in agreement with DFT computation. Moreover, the Mo EXAFS rGO/MoO_2 structural data are consistent with isolated $(C\text{-}O)_2\text{-}Mo(=O)_2$ species having two Mo=O bonds and two Mo-O bonds at distances of 1.69 Å and 1.90 Å, respectively. rGO/MoO_2 is also more active than the previously reported AC/MoO_2 catalyst, with reductive carbonyl coupling TOFs approaching 1814 h^{-1}. rGO/MoO_2 is environmentally robust and multiply recyclable with 69 ± 2% of the Mo sites catalytically significant. Overall, rGO/MoO_2 is a structurally well-defined and versatile single-site Mo(VI) dioxo heterogeneous catalytic system.

INTRODUCTION

Catalysis is central to many industrial sectors including energy, healthcare, transportation, environment, etc., with over 80% of industrial processes involving at least one catalytic step.[1] By virtue of the high stability and recyclability, heterogeneous catalysts dominate large-scale commercial processes. However, detailed structural understanding of these substances has been challenged by the complexity and wide variety of surface sites possible or thought to be present. Therefore, an important goal in heterogeneous catalysis is to rationally create well-defined catalytically active sites for enhanced atom efficiency, catalytic selectivity, and simplified mechanistic analysis. To address this challenge, single-site heterogeneous catalysts (SSHCs) derived from molecular precursors with well-dispersed metal centers on solid supports offer an attractive means to bridge the homogeneous-heterogeneous catalysis gap.[2-12]

Molybdenum plays important roles in mediating numerous catalytic transformations, ranging from elaborate metalloenzyme systems to large-scale industrial processes,[13] and high-valent oxo-molybdenum complexes serve as excellent catalysts in numerous laboratory-scale oxidation and reduction reactions.[14-15] Furthermore, immobilizing solution phase MoO_x complexes on supports affords active heterogeneous catalysts,[16-17] and SSHC has been used to prepare high activity silica-supported Mo oxo alkylidene olefin metathesis catalysts.[18-19] In comparison to many conventional refractory oxide supports, carbon materials can have high surface areas, low cost, good thermal stability, tunable surface functionality, and varying degrees of structural regularity, providing versatile supports in conventional heterogeneous catalysis, as well as intriguing candidates for exploratory SSHC research.[20-21] Recently, this Laboratory reported the first single-site molybdenum dioxo catalyst supported on activated carbon, AC/MoO_2 (Scheme 1).[22] This catalyst was prepared via grafting of a molecular $(dme)MoO_2Cl_2$ precursor onto activated carbon. AC/MoO_2 was characterized by N_2 physisorption, H_2-TPR, ICP, and EXAFS. It is air- and moisture-stable, multiply recyclable, and exhibits

Scheme 1. Tentative structures for and comparison between AC/MoO_2 and rGO/MoO_2 single-site heterogeneous catalysts.

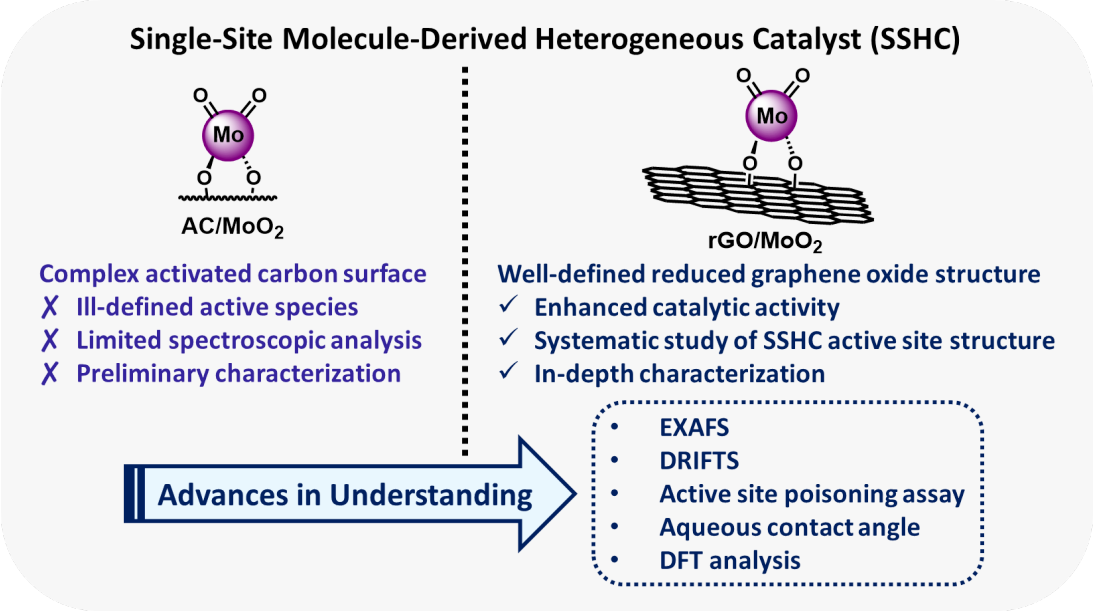

remarkable catalytic activity and selectivity in trans-esterification,[22] alcohol dehydrogenation,[23] reductive carbonyl coupling,[24] *N*-oxide reduction,[25] and high-yield solvent-free polyethylene terephthalate (PET) deconstruction.[26] Nevertheless, activated carbon has been categorized as an ill-defined carbon source since many details of the structure remain obscure.[27-28] Therefore, while AC/MoO_2 demonstrates versatile reactivity, the structurally near-amorphous/heterogeneous and optically absorptive nature of activated carbon has impeded many characterization techniques normally available to SSHC structural studies. As a result, an in-depth understanding of the catalytic sites of this intriguing AC/MoO_2 system, including the percentage of sites which are catalytically significant, remains uncertain. Furthermore catalysts based on activated carbons tend to exhibit unpredictable reproducibility due to the variability of carbon precursor compositions.[29]

To explore the scope of Carbon/MoO_2 catalysis and to develop a better-defined structure-activity-selectivity description of the AC/MoO_2 surface sites, alternative structurally better-defined carbon supports are of obvious interest. We recently reported the synthesis of an exotic "carbon nanohorn" supported Mo dioxo catalyst (CNH/MoO_2) prepared via an analogous synthetic approach to AC/MoO_2 but in mg quantities.[30] CNH/MoO_2 was characterized by single-molecule atomic-resolution real-time electron microscopy (SMART-EM) at the University of Tokyo, providing the first atomistic model for MoO_2 species binding to a graphitic surface, and in an out-of-plane mode. The measurable catalytic function of CNH/MoO_2 suggests a tentative but qualitative model for Carbon/MoO_2 species. Nevertheless, more detailed metrical information will be necessary to make meaningful structure-adsorbate catalytic activity/selectivity correlations for advancing this field.

Graphene-based materials, such as graphene oxide (GO) and reduced graphene oxide (rGO), are generally classified as well-defined carbon sources with uniform hybridization and long-range order.[27] They are composed of single or multilayers of graphene-like sheets, and thus are far more structurally regular than AC. Furthermore, GO and rGO have recently been tested as supports for conventional heterogeneous catalysis,[31-32] and exhibit tunable surface functionality characterizable by DRIFTS and Raman vibrational spectroscopy.[33-35] Therefore, supporting Mo dioxo complexes on graphitic materials may afford single-site catalysts with informative spectroscopic/structural and catalytic performance properties. Here we describe the realization of a novel reduced graphene oxide (rGO) supported single-site molybdenum dioxo catalyst (rGO/MoO_2; Scheme 1). rGO/MoO_2 is characterized by XPS, DRIFTS, powder XRD, N_2 physisorption, NH_3-TPD, aqueous contact angle, active site assay poisoning, Mo EXAFS, model compound single-crystal XRD, DFT computation, and catalytic reactions. It will be seen that the EXAFS, DFT, molecular model compound metrical, and vibrational spectroscopic data uniquely converge on a coordinatively-unsaturated four-coordinate Mo center with two single -CO-Mo bonds and two Mo=O multiple bonds. In reductive carbonyl coupling at a TOF of 1814 h^{-1}, rGO/MoO_2 is multiply recyclable with 69 ± 2% of the Mo sites catalytically significant. The use of rGO in this study strongly enhances the fundamental understanding of carbon-supported MoO_2 catalysts and their chemistry, and the present synthetic and experimental/theoretical characterization approach will serve as a model for studies of other single-site heterogeneous catalysts.

RESULTS AND DISCUSSION

Synthesis and Characterization of (dme)MoO_2Cl_2. The (dme)MoO_2Cl_2 precursor was prepared from commercially available MoO_2Cl_2 and dimethoxyethane,[36] with purity confirmed by solution phase NMR spectroscopy and elemental analysis (Figure S1; Table S1). Diffraction-quality (dme)MoO_2Cl_2 single crystals were grown from CH_2Cl_2 to obtain precise structural data (Figure 1a). In contrast to the 298 K structure determined decades ago,[37]

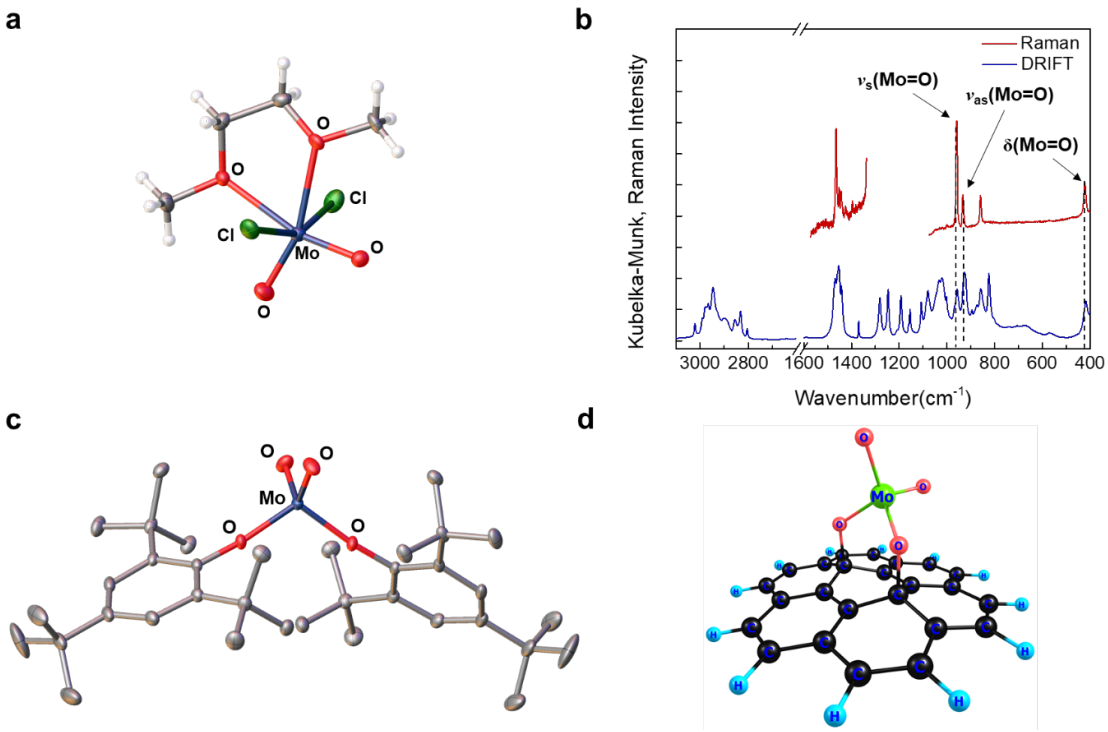

Figure 1. Structural characterization of precursor (dme)MoO_2Cl_2, model compound [(2,4,6-tri-^{t}Bu)C_6H_2O]$_2MoO_2$, and catalyst rGO/MoO_2. (**a**) Crystal structure of (dme)MoO_2Cl_2 precursor. Blue = Mo, red = O, green = Cl, grey = C, white = H. (**b**) DRIFT and near-IR Raman spectra of (dme)MoO_2Cl_2 precursor. (**c**) Crystal structure of [(2,4,6-tri-^{t}Bu)C_6H_2O]$_2MoO_2$ model compound. Blue = Mo, red = O, grey = C. Selected atoms are labeled, and H atoms are omitted for clarity. (**d**) DFT model of rGO/MoO_2 structure. Green = Mo, red = O, black = C, blue = H.

Table 1. Comparison of experimental vibrational spectroscopic, EXAFS, single-crystal XRD, and DFT computed structural data, for precursor (dme)MoO_2Cl_2, model compound [(2,4,6-tri-^{t}Bu)C_6H_2O]$_2MoO_2$, and catalyst rGO/MoO_2.

Entry	Sample	Bond Type	Bond Number	Vibrational Frequency (cm^{-1})		Bond Length (Å)		
				DRIFTS	DFT	EXAFS	Single-Crystal XRD	DFT
1	(dme)MoO_2Cl_2	Mo=O	2	958 ; 933	963 ; 947	1.70(2)	1.682(3) ; 1.691(3)	1.71
2	[(2,4,6-tri-^{t}Bu)C_6H_2O]$_2MoO_2$	Mo=O	2	962[a] ; 937[a]	949 ; 931	1.70(2)	1.6934(8)	1.72
		Mo-O	2	880[a]	882 ; 878	1.88(2)	1.8572(7)	1.88
3	rGO/MoO_2	Mo=O	2	959 ; 927	970 ; 951	1.69(3)	N/A	1.71 ; 1.72
		Mo-O	2	732	776 ; 738	1.90(3)	N/A	1.91

[a] Experimental vibrational frequencies obtained from transmission IR spectroscopy.

the present 100 K data minimize thermal motion, dynamic disorder, and reduce radiation damage to yield more accurate metrical data.[38] The Mo=O bond lengths of 1.682(3) Å and 1.691(3) Å, together with the O=Mo=O bond angle of 104.86(17) °, indicate a *cis*-MoO_2 configuration. For (DRIFTS) and near-IR Raman spectroscopy were also used to characterize the MoO_2 fragment (Figure 1b). Powders were examined in an N_2-purged DRIFTS cell to avoid ambient exposure during data collection. Similarly, an in-situ Raman cell was used to avoid exposure to ambient air during the Raman measurements excited at 780 nm.[39] Both experiments detect three features at 958 cm^{-1}, 933 cm^{-1}, and 422 cm^{-1}, which are assignable to the symmetric and *anti*-

more detailed information, see Table S2. These data are in excellent agreement with EXAFS and DFT results, which indicate Mo=O distances of 1.70(2) Å and 1.71(2) Å, respectively (Table 1).

Diffuse reflectance IR Fourier transform spectroscopy symmetric O=Mo=O stretching modes and O=Mo=O bending mode, respectively, typical of a bent O=Mo=O fragment.[40] The DFT calculations yield Mo=O bond lengths of 1.71 Å, and stretching and bending modes of 963 cm^{-1}, 947 cm^{-1}, and 390 cm^{-1}, respectively, in excellent accord with the experimental X-ray, EXAFS, and vibrational spectroscopic data (Table 1).

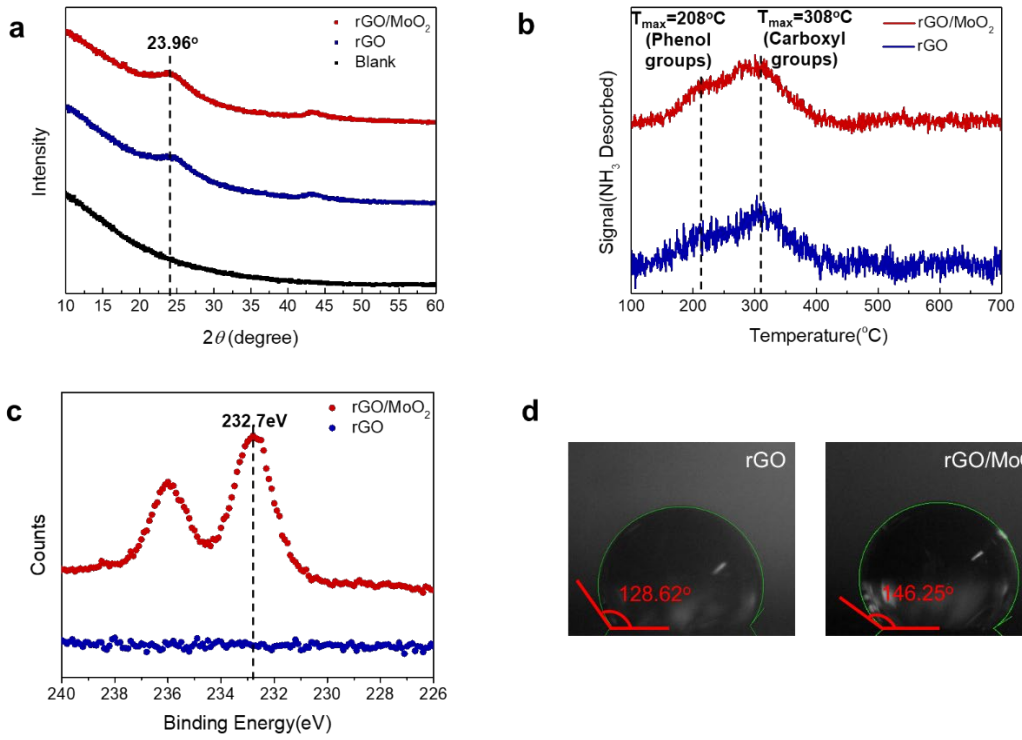

Figure 2. Characterization of rGO and rGO/MoO_2. (**a**) PXRD patterns of rGO (blue) and rGO/MoO_2 (red) using Cu Kα X-rays. (**b**) NH_3-TPD traces of rGO (blue) and rGO/MoO_2 (red). (**c**) XPS Mo 3d ionizations of rGO (blue) and rGO/MoO_2 (red). (**d**) Advancing aqueous contact angle images of rGO (left) and rGO/MoO_2 (right).

Table 2. Summary of BET surface area, PXRD, NH_3-TPD, and aqueous contact angle data for rGO and rGO/MoO_2.

Entry	Material	BET Surface Area (m^2/g)	PXRD Peak 2θ (°)	NH_3-TPD Peak (°C)	Aqueous Contact Angle (°)
1	rGO	179	23.96	208 ; 308	128.62
2	rGO/MoO_2	127	23.96	208 ; 308	146.25

Synthesis and Characterization of GO and rGO. Graphene oxide (GO) was synthesized from graphite using a modified Hummers procedure,[41] and was washed with acid and acetone to avoid gelation.[42] XPS analysis shows that GO has high oxygen content (Figure S2). It is composed of 61.0 at% C and 37.6 at% O, as well as minor S impurities. Note that the presence of dense functional groups may complicate the Mo precursor adsorption process. For example, if three or more OH groups were located in close proximity, the precursor might aggregate, compromising the formation of single sites. Therefore, thermal reduction was used to remove redundant GO oxygen-containing functional groups to afford reduced graphene oxide (rGO) with good stability.[43-44] XPS analysis shows that the present rGO has lower O content with a significantly higher percentage of aromatic C=C groups than GO. An XPS survey scan shows the present rGO is composed of 85.1 at% C and 14.9 at% O (Figure S3). This should be sufficient as the previous activated carbon (AC) support had ca 5.2 at% O content.[22] The present C 1s spectrum can be resolved into four component peaks, corresponding to C-C/C=C, C-O, C=O, and a π-π* satellite observed at 284.6 eV, 286.1 eV, 288.1 eV, and 291.8 eV, respectively (Figure S3).[43, 45] Notably, the π-π* satellite feature indicates significant delocalized π conjugation; therefore, it is reasonable that the thermal reduction restores some of the aromatic characters.[46] This aromatic feature has not been observed in the C 1s spectrum of activated carbon, which further underscores that rGO has a more regular structure than AC (Table S6).

UV Raman spectroscopy was next used to probe the rGO structure defects (Figure S4). The 1588 cm^{-1} G band originates from in-plane vibrations of sp^2 C atoms, while the D band at 1391 cm^{-1} is attributable to defects, vacancies, and sp^2 domain distortions.[47] The integrated intensity ratio of D/G bands is 1.45. From the PXRD data, rGO displays a (002) reflection at 2θ = 23.96 °, indicating a lattice spacing of ~3.71 Å (Figure 2a).[43, 48] Notably, AC has a broader peak at 2θ = 24.14 °, which indicates that it has a less ordered structure/shorter coherence length than rGO (Figure S9). A comparative summary of characterization results for AC and rGO can be found in Table S6. NH_3-TPD experiments were next performed to better characterize the rGO surface sites (Figure 2b). T_{max} features are observed at 208 °C and 308 °C, likely attributable to the presence of phenolic and carboxyl groups, respectively.[49-50] The rGO BET surface area by N_2 physisorption is 179 m^2/g. Overall, these data verify

that thermal processing successfully provides rGO with low but sufficient surface OH sites for potential catalyst binding.

Synthesis and Characterization of rGO/MoO_2. To prepare rGO/MoO_2, direct grafting of the precursor onto rGO was employed. According to ICP-OES, rGO/MoO_2 synthesized in this way has 1.3 wt% Mo loading, corresponding to ~0.64 Mo/nm^2. The XPS C 1s spectrum of rGO/MoO_2 remains essentially unchanged from the starting rGO (Figure S5). Note however that a new Mo3$d_{5/2}$ feature is observed at 232.7 eV, indicating the presence of a bound Mo^{VI} species (Figure 2c).[22, 51] Furthermore, no metal-Cl is detected in rGO/MoO_2, supporting the grafting mechanism in which (dme)MoO_2Cl_2 precursor reacts with rGO surface -OH groups via protonolysis of the Mo-Cl bonds, yielding the supported catalyst and releasing (dme) as well as HCl. Small amounts of organic-Cl are detected, presumably due to chemisorption of Cl^- on the rGO surface (Figure S5).[52-53] The proposed grafting mechanism is supported by DFT computation which includes two subsequent low-barrier ($\Delta G^{\ddagger}$ <20 kcal/mol) HCl eliminations steps (Scheme S1). Similar PXRD patterns are observed for rGO and rGO/MoO_2, indicating negligible changes in lattice spacing for the ordered graphitic regions, implying that MoO_2 adsorption does not significantly interfere with the interplanar stacking, presumably because it is located in less ordered regions or on graphitic plane edges (Figure 2a). There is no evidence for discrete crystalline MoO_x species according to the PXRD pattern since no corresponding peaks are observed.[54] The BET surface area is 127 m^2/g for rGO/MoO_2. Mo grafting may block some rGO surface defect sites or pores, causing the observed contraction in surface area (Table S3).[55] NH_3-TPD traces of rGO/MoO_2 are similar to those of pristine rGO, neither shifting the T_{max} values nor creating additional events (Figure 2b). This indicates that the anchored rGO/MoO_2 surface, which is the catalytically active species (control experiments show that rGO has negligible activity), does not have strong acidity. Quantitation based on the NH_3-TPD traces shows that the overall acidic surface site density is reduced upon grafting of Mo, supporting the previously proposed grafting mechanism (Table S4). Advancing aqueous contact angle analysis was performed to assess any changes in rGO surface hydrophilicity resulting from the Mo grafting (Figure 2d).[56] rGO/MoO_2 has an aqueous contact angle of 146.25 °, significantly greater than that of rGO, 128.62 °, and indicating a more hydrophobic surface. With modern instrumentation, the uncertainty in contact angle measurements is generally considered to be ≤ ± 2 °.[57] Comparative rGO - rGO/MoO_2 characterization data are summarized in Table 2. Overall, MoO_2 grafting likely consumes acidic/polar surface sites but does not significantly change the well-defined rGO bulk structure.

rGO/MoO_2 Vibrational Spectroscopy. DRIFTS was employed to better characterize the bound *cis*-Mo(=O)$_2$ moiety (Figure S6). Besides νC=O (1752 cm^{-1}), νC=C (1583 cm^{-1}), and νC-O (1238 cm^{-1}) modes from the support, rGO/MoO_2 exhibits two features at 959 cm^{-1} and 927 cm^{-1}, assignable to the symmetrically and *anti*-symmetrically coupled Mo=O stretching modes of a *cis*-(O=Mo=O) moiety, in good agreement with the aforementioned (dme)MoO_2Cl_2 precursor features at 958 cm^{-1} and 933 cm^{-1} (Figure 1b). Similar values are obtained for other simple and supported *cis*-dioxo-Mo complexes such as mononuclear [(2,4,6-tri-^{t}Bu)C_6H_2O]$_2MoO_2$ (Figure 1c).[58-59] The 732 cm^{-1} feature is tentatively assigned to a Mo-O single bond stretch of rGO/MoO_2. Moreover, these data are in good agreement with DFT results (Table 1). Notably, this is the first identification of Mo=O/Mo-O features in Carbon/MoO_2 catalyst vibrational spectra.

rGO/MoO_2 EXAFS. Mo K-edge EXAFS was next used to investigate the structure of the supported catalyst. The fitting results reveal that rGO/MoO_2 has two Mo=O bond distances of 1.69(3) Å and two Mo-O bond distances of 1.90(3) Å , (Table 1; Figure S8). rGO/MoO_2 and AC/MoO_2 have very similar active-site structures, and thus it is reasonable to assume that rGO/MoO_2 can serve as a representative model for this Carbon/MoO_2 catalytic system. Notably, the EXAFS fit for rGO/MoO_2 is significantly improved when compared to AC/MoO_2, as the raw spectrum for AC/MoO_2 could not be fit directly and the structure of the catalyst was derived from a difference spectrum (Table S5; Table S7).[22] Furthermore, the EXAFS metrical data are in excellent agreement with those of the model compounds in Figure 1c as well as the DFT results (Table 1). Moreover, the EXAFS data show that the catalyst structure is unchanged upon heating overnight at 150 °C, demonstrating the thermal stability of rGO/MoO_2 (Table S5).

rGO/MoO_2 Model Compound Structure. To obtain a further understanding of the rGO/MoO_2 structure, [(2,4,6-tri-^{t}Bu)C_6H_2O]$_2MoO_2$ was chosen as a model. This compound was synthesized according to the literature procedure.[59] Although a crystal structure was previously reported for "green" crystals of this substance,[59] the yellow-orange crystals we obtained prompted a reinvestigation. The four-coordinate isostructural geometry (Figure 1c) has two Mo=O bond distances of 1.6934(8) Å and two Mo-O bond distances of 1.8572(7) Å, in accord with the experimental EXAFS and computed DFT results (Table 1). Furthermore, the O=Mo=O bond angle is 105.90(6) °, indicating a *cis*-MoO_2 configuration (see Table S8 for more information). According to transmission IR spectroscopy, the model compound has two Mo=O stretches at 962 cm^{-1} and 937 cm^{-1}, and a Mo-O stretch at 880 cm^{-1}, all of which align well with the DFT calculations (Table 1; t10). Comparing the vibrational frequencies and bond lengths of the model compound to that of rGO/MoO_2, it can be concluded that there is a very strong similarity (Table 1), and that this well-defined four-coordinate model further supports the proposed rGO/MoO_2 catalyst structure.

DFT Computation. To complement the experimental results, DFT calculations were carried on an rGO/MoO_2 model (Figure 1d). The structure and frequencies were computed at the same level as for the (dme)MoO_2Cl_2 complex, which gave excellent agreement with experimental results (see SI for details). The calculations reveal that rGO/MoO_2 has two Mo=O stretches at 970 cm^{-1} and 951 cm^{-1}, and two Mo-O stretches at 776 cm^{-1} and 738 cm^{-1}, in good agreement with the DRIFTS results (Table 1). Furthermore, rGO/MoO_2 has two 1.71 Å/1.72 Å Mo=O bonds and two 1.91 Å Mo-O bonds, in good agreement with the EXAFS and model compound diffraction data (Table 1). To show that the present DFT model is generally applicable,

Table 3. Comparison of catalytic activities of rGO/MoO_2 and AC/MoO_2.

Entry	Reaction	Catalyst	Mo (mol %)	Time (min)	Conv. (%)	TOF (h^{-1})
1	Reductive carbonyl coupling	rGO/MoO_2	0.1	15	31.3	$1.81x10^{3}$ [a]
		AC/MoO_2	0.1	60	24.7	494[b]
2	*N*-oxide reduction	rGO/MoO_2	2	10	15.0	65[a]
		AC/MoO_2	2	55	33.3	36[b]

[a] TOF calculated assuming 69% active sites.
[b] TOF calculated assuming 50% active sites.[22]

Scheme 2. (a) Reductive carbonyl coupling of benzaldehyde. (b) Reduction of 2-methyl pyridine *N*-oxide.

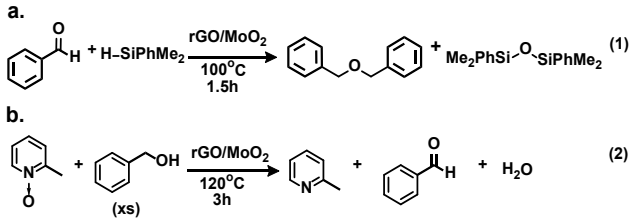

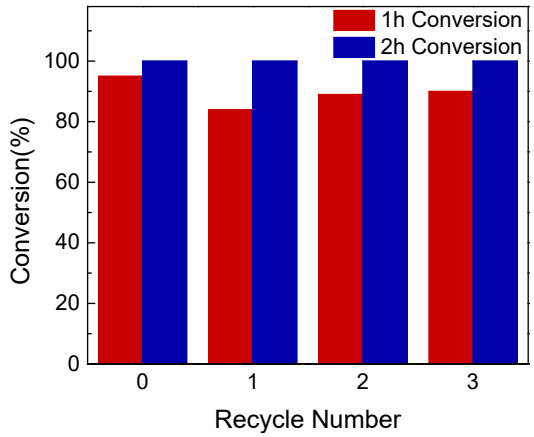

Figure 3. rGO/MoO_2 catalyzed reductive carbonyl coupling recycling test. The consistent conversion of benzaldehyde to dibenzyl ether after 1 h (red) and 2 h (blue) reaction time supports the robustness of rGO/MoO_2.

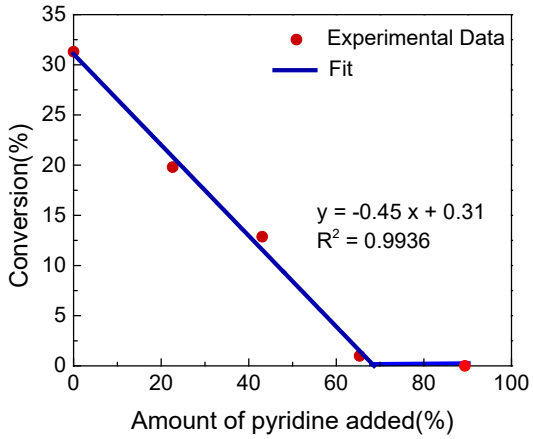

Figure 4. Pyridine poisoning titration of rGO/MoO_2-catalyzed benzaldehyde reductive carbonyl coupling. The linear decrease of 15 min conversion as a function of the amount of pyridine titrated and the x-axis intercept yield 69 ± 2% active sites.

additional calculations were carried out using a larger graphene sheet. Identical Mo-O and Mo=O bond distances are computed using the new model, demonstrating that adequate carbon atom numbers were included in the previous model. The Mo-O/Mo=O vibrational frequencies of the new model (Mo-O stretches at 729 cm^{-1} & 746 cm^{-1}; Mo=O stretches at 948 cm^{-1} and 965 cm^{-1}) are also very similar to the experimental and calculated values for the previous model shown in Figure 1d. Furthermore, the Mo-C interaction is detected via Mo-EXAFS, and the experimental bond length is in the range of 3.1-3.3 A, which is in good agreement with the current and previous DFT model, indicating that sufficient carbon atoms are included in the present DFT model.

rGO/MoO_2 Catalysis. While the above results provide a plausible structural description of the Carbon/MoO_2 single-site catalyst, the question remains as to whether it is an accurate functional model. Therefore, rGO/MoO_2 was investigated for the reductive carbonyl coupling with silanes and 2-methyl pyridine *N*-oxide reduction with an alcohol, for which AC/MoO_2 is highly competent (Scheme 2).[24-25] In catalytic experiments under identical conditions to those reported for AC/MoO_2, eq. 1 affords 100% conversion to dibenzyl ether after 1.5 h, and eq. 2 affords 100% conversion to methyl pyridine after 3 h. Normalizing for the different Mo coverages of rGO/MoO_2 and AC/MoO_2, kinetic measurements reveal that the rGO/MoO_2 turnover frequencies for both eqs 1 and 2 are greater than the AC/MoO_2 turnover frequencies (Table 3). Furthermore, recycling experiments show that rGO/MoO_2 can be recycled at least 3 times without significant decline in activity (Figure 3). The recycled catalyst shows similar Mo $3d_{5/2}$ features and Mo loading compared to the raw catalyst according to XPS and ICP-OES,[60] respectively, supporting the high stability of the grafted Mo species. (Figure S11).

Active Site Assay. The density of catalytically significant sites was estimated with a pyridine poisoning titration. Lewis basic pyridine is expected to coordinate to unoccupied orbitals of the electrophilic Mo(VI) center, and to poison catalytic activity. As the Mo-dioxo sites are successively poisoned over the course of the titration, catalytic activity is anticipated to decline. Therefore, the catalytically significant rGO/MoO_2 sites should be quantifiable by the equiv. of poison required to suppress activity. The use of pyridine has previously been reported to poison Lewis acidic catalysts.[61-64] In the present assay, 15 min conversions of benzaldehyde were monitored as increasing equivalents of pyridine were titrated into the reaction mixture (Figure 4). Linear responses suggest that

the poison reacts with the active sites uniformly and proportionately, and extrapolation to zero benzaldehyde conversion indicates that 69 ± 2% of the Mo sites are catalytically significant. This percentage is quite high when compared to literature reported supported MoO_x catalysts, which typically have <2 % surface active sites.[65-66] In addition to single-Mo sites, we speculate that there may exist single Mo sites with similar but catalytically deactivating binding modes or multi-Mo sites in the catalytic system having very different chemical properties. Such multi-Mo sites may also not be catalytically significant, and thus would not affect the linear response in the poisoning assay. Furthermore, catalysis is also dependent on the coordination sphere, such as the differences introduced by the carbon geometry or other functionalities,[67] which also explains why the well-organized rGO support yields a higher percentage of active sites than AC which is less-ordered. By XPS analysis, the completely poisoned catalyst has a Mo : N ratio of 1 : 1, suggesting that any other Mo sites present do not readily react with pyridine (Figure S12). Moreover, according to the DFT calculations, pyridine coordination to rGO/MoO_2 is energetically favored by ~3.9 kcal/mol over benzaldehyde coordination, supporting the efficacy of pyridine as an effective poison for the rGO/MoO_2-mediated reductive coupling of benzaldehyde (Scheme 3).

Scheme 3. DFT-computed competitive coordination of pyridine and benzaldehyde to rGO/MoO_2, arguing that pyridine coordination is more stable than that of benzaldehyde.

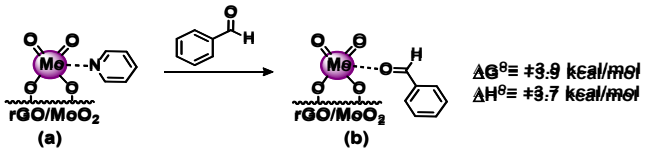

CONCLUSIONS

The graphitic carbon-supported single-site catalyst, rGO/MoO_2, was synthesized and characterized in detail both experimentally and computationally. Grafting of MoO_2 consumes surface polar sites of the rGO surface according to aqueous contact angle analysis. Experimental Mo=O vibrational frequencies are observed at 959 cm^{-1} and 927 cm^{-1} via DRIFTS; Mo=O and Mo-O bond lengths of 1.69(3) Å and 1.90(3) Å, respectively, are obtained from EXAFS. These experimental data align well with DFT computational results as well as model compound single-crystal diffraction data, affording detailed structural understanding of single-site Carbon/MoO_2 catalysts and demonstrating their potential in future catalyst design, new reaction modalities, and structure-function studies. Furthermore, rGO/MoO_2 exhibits catalytic activity in reductive carbonyl coupling and *N*-oxide reduction reaction rivaling or exceeding that of previously reported AC/MoO_2, which mediates a broad scope of oxygenate transformations. According to a poisoning assay, rGO/MoO_2 has 69 ± 2% catalytically significant Mo sites. Overall, rGO/MoO_2 shows promise as a well-defined, efficient, and scalable catalytic system.

ASSOCIATED CONTENT

Supporting Information

The Supporting Information is available free of charge on the ACS Publications website. Experimental details, physical and analytical measurements, characterization results, procedures for catalytic reactions, DFT calculations, including Tables S1-S8 and Figures S1-S12.

Accession Codes

CCDC 2077947 and 2077942 contain the supplementary crystallographic data for this paper. These data can be obtained free of charge via www.ccdc.cam.ac.uk/data_request/cif, or by emailing data_request@ccdc.cam.ac.uk, or by contacting The Cambridge Crystallographic Data Centre, 12 Union Road, Cambridge CB2 1EZ, UK; fax: +44 1223 336033.

AUTHOR INFORMATION

Corresponding Authors

Tobin J. Marks – Department of Chemistry and the Institute for Catalysis in Energy Processes (ICEP), Northwestern University, Evanston, Illinois 60208, United States.

orcid.org/0000-0001-8771-0141

E-mail: t-marks@northwestern.edu

Yosi Kratish – Department of Chemistry and the Institute for Catalysis in Energy Processes (ICEP), Northwestern University, Evanston, Illinois 60208, United States.

Email: yosi.kratish@northwestern.edu

Michael J. Bedzyk – Department of Material Science and Engineering and the Institute for Catalysis in Energy Processes (ICEP), Northwestern University, Evanston, Illinois 60208, United States.

orcid.org/0000-0002-1026-4558

Email: bedzyk@northwestern.edu

George C. Schatz – Department of Chemistry and the Institute for Catalysis in Energy Processes (ICEP), Northwestern University, Evanston, Illinois 60208, United States.

orcid.org/0000-0001-5837-4740

Email: g-schatz@northwestern.edu

Authors

Yiqi Liu – Department of Chemistry and the Institute for Catalysis in Energy Processes (ICEP), Northwestern University, Evanston, Illinois 60208, United States.

Jiaqi Li – Department of Chemistry and the Institute for Catalysis in Energy Processes (ICEP), Northwestern University, Evanston, Illinois 60208, United States.

Anusheela Das – Department of Material Science and Engineering and the Institute for Catalysis in Energy Processes (ICEP), Northwestern University, Evanston, Illinois 60208, United States.

Hacksung Kim – Center for Catalysis and Surface Science, Northwestern University, Evanston, Illinois 60208, United States and Chemical Sciences and Engineering Division, Argonne National Laboratory, Lemont, Illinois 60439, United States. **orcid.org/**0000-0002-5599-065X

Leighton O. Jones – Department of Chemistry and the Institute for Catalysis in Energy Processes (ICEP), Northwestern University, Evanston, Illinois 60208, United States. **orcid.org/0000-0001-6657-2632**

Qing Ma – DND - CAT, Northwestern Synchrotron Research Center at the Advanced Photon Source, Argonne National Laboratory, Lemont, Illinois 60439, United States.

Author Contributions

‡Y.L. and J.L contributed equally to this work. The manuscript was written through contributions of all authors. All authors have given approval to the final version of the manuscript.

Notes

The authors declare no competing financial interest.

ACKNOWLEDGMENT

Financial support was provided by the U.S. Department of Energy, Office of Science, Office of Basic Energy Sciences under Award Number DOE DE-FG02-03ER15457 to the Institute for Catalysis in Energy Processes (ICEP) at Northwestern University (NU). This work made use of IMSERC facilities at NU, which have received support from Soft and Hybrid Nanotechnology Experimental (SHyNE) Resource (NSF ECCS-2025633), Int. Institute of Nanotechnology (IIN), and NU. This work made use of the NU QBIC supported by NASA Ames Research Center Grant NNA04CC36G. This work made use of the Keck-II and XRD facilities at NU supported by SHyNE, NSF-MRSEC program (DMR-1720139), and IIN. This work made use of the REACT Facility of NU's Center for Catalysis and Surface Science supported by a grant from the DOE (DE-SC0001329). This work used the DuPont-Northwestern-Dow Collaborative Access Team (DND-CAT) 5BM-D beamline at the Advanced Photon Source (APS). DND-CAT is supported by NU, E. I. DuPont de Nemours & Co., and The Dow Chemical Company. The APS is supported by DOE at Argonne National Laboratory under Contract No. DE-AC02-06CH11357. This research was supported in part by the computational resources and staff contributions provided by the Quest High Performance Computing Facility at NU, which is jointly supported by the Office of the Provost, the Office for Research, and NU Information Technology. We thank C. L. Stern of IMSERC, S. Alayoglu and N. M, Schweitzer of REACT, A. M. Arinaga and Dr. Y. Gao of NU, Dr. Alexander Kaushansky of the Technion Israel Institute of Technology for helpful insights and discussions.

REFERENCES

1. Wang, A.; Li, J.; Zhang, T., Heterogeneous single-atom catalysis. *Nature Reviews Chemistry* **2018,** *2* (6), 65-81.

2. Chen, E. Y. X., Coordination Polymerization of Polar Vinyl Monomers by Single-Site Metal Catalysts. *Chemical Reviews* **2009,** *109* (11), 5157-5214.

3. Copéret, C.; Allouche, F.; Chan, K. W.; Conley, M. P.; Delley, M. F.; Fedorov, A.; Moroz, I. B.; Mougel, V.; Pucino, M.; Searles, K.; Yamamoto, K.; Zhizhko, P. A., Bridging the Gap between Industrial and Well-Defined Supported Catalysts. *Angewandte Chemie International Edition* **2018,** *57* (22), 6398-6440.

4. Copéret, C.; Comas-Vives, A.; Conley, M. P.; Estes, D. P.; Fedorov, A.; Mougel, V.; Nagae, H.; Núñez-Zarur, F.; Zhizhko, P. A., Surface Organometallic and Coordination Chemistry toward Single-Site Heterogeneous Catalysts: Strategies, Methods, Structures, and Activities. *Chemical Reviews* **2016,** *116* (2), 323-421.

5. Eisen, M. S.; Marks, T. J., Supported organoactinide complexes as heterogeneous catalysts. A kinetic and mechanistic study of facile arene hydrogenation. *Journal of the American Chemical Society* **1992,** *114* (26), 10358-10368.

6. LiBretto, N. J.; Xu, Y.; Quigley, A.; Edwards, E.; Nargund, R.; Vega-Vila, J. C.; Caulkins, R.; Saxena, A.; Gounder, R.; Greeley, J.; Zhang, G.; Miller, J. T., Olefin oligomerization by main group Ga3+ and Zn2+ single site catalysts on SiO2. *Nature Communications* **2021,** *12* (1), 2322.

7. Luo, Q.-X.; Zhang, Y.-B.; Qi, L.; Scott, S. L., Glucose Isomerization and Epimerization over Metal-Organic Frameworks with Single-Site Active Centers. *ChemCatChem* **2019,** *11* (7), 1903-1909.

8. Peters, B.; Scott, S. L., Single atom catalysts on amorphous supports: A quenched disorder perspective. *The Journal of Chemical Physics* **2015,** *142* (10), 104708.

9. Stalzer, M. M.; Delferro, M.; Marks, T. J., Supported Single-Site Organometallic Catalysts for the Synthesis of High-Performance Polyolefins. *Catalysis Letters* **2015,** *145* (1), 3-14.

10. Thomas, J. M.; Raja, R.; Lewis, D. W., Single-Site Heterogeneous Catalysts. **2005,** *44* (40), 6456-6482.

11. Tilley, T. D., Molecular design and synthesis of heterogeneous and single-site, supported catalysts. *Journal of Molecular Catalysis A: Chemical* **2002,** *182-183*, 17-24.

12. Wegener, S. L.; Marks, T. J.; Stair, P. C., Design Strategies for the Molecular Level Synthesis of Supported Catalysts. *Accounts of Chemical Research* **2012,** *45* (2), 206-214.

13. Schwarz, G.; Mendel, R. R.; Ribbe, M. W., Molybdenum cofactors, enzymes and pathways. *Nature* **2009,** *460* (7257), 839-847.

14. Hernández-Ruiz, R.; Sanz, R., Dichlorodioxomolybdenum(VI) Complexes: Useful and Readily Available Catalysts in Organic Synthesis. *Synthesis* **2018,** *50* (20), 4019-4036.

15. Karunadasa, H. I.; Chang, C. J.; Long, J. R., A molecular molybdenum-oxo catalyst for generating hydrogen from water. *Nature* **2010,** *464* (7293), 1329-1333.

16. Chakrabarti, A.; Wachs, I. E., Molecular Structure–Reactivity Relationships for Olefin Metathesis by Al2O3-Supported Surface MoOx Sites. *ACS Catalysis* **2018,** *8* (2), 949-959.

17. Shetty, M.; Murugappan, K.; Green, W. H.; Román-Leshkov, Y., Structural Properties and Reactivity Trends of Molybdenum Oxide Catalysts Supported on Zirconia for the Hydrodeoxygenation of Anisole. *ACS Sustainable Chemistry & Engineering* **2017,** *5* (6), 5293-5301.

18. Merle, N.; Le Quéméner, F.; Bouhoute, Y.; Szeto, K. C.; De Mallmann, A.; Barman, S.; Samantaray, M. K.; Delevoye, L.; Gauvin, R. M.; Taoufik, M.; Basset, J.-M., Well-Defined Molybdenum Oxo Alkyl Complex Supported on Silica by Surface Organometallic Chemistry: A Highly Active Olefin Metathesis Precatalyst. *Journal of the American Chemical Society* **2017,** *139* (6), 2144-2147.

19. Pucino, M.; Zhai, F.; Gordon, C. P.; Mance, D.; Hoveyda, A. H.; Schrock, R. R.; Copéret, C., Silica-Supported Molybdenum Oxo Alkylidenes: Bridging the Gap between Internal and Terminal Olefin Metathesis. *Angewandte Chemie International Edition* **2019,** *58* (34), 11816-11819.

20. Gerber, I. C.; Serp, P., A Theory/Experience Description of Support Effects in Carbon-Supported Catalysts. *Chemical Reviews* **2020,** *120* (2), 1250-1349.

21. Lam, E.; Luong, J. H. T., Carbon Materials as Catalyst Supports and Catalysts in the Transformation of Biomass to Fuels and Chemicals. *ACS Catalysis* **2014,** *4* (10), 3393-3410.

22. Mouat, A. R.; Lohr, T. L.; Wegener, E. C.; Miller, J. T.; Delferro, M.; Stair, P. C.; Marks, T. J., Reactivity of a Carbon-Supported Single-Site Molybdenum Dioxo Catalyst for Biodiesel Synthesis. *ACS Catal.* **2016,** *6* (10), 6762-6769.

23. Lohr, T. L.; Mouat, A. R.; Schweitzer, N. M.; Stair, P. C.; Delferro, M.; Marks, T. J., Efficient catalytic greenhouse gas-free hydrogen and aldehyde formation from aqueous alcohol solutions. *Energy & Environmental Science* **2017,** *10* (7), 1558-1562.

24. Liu, S.; Li, J.; Jurca, T.; Stair, P. C.; Lohr, T. L.; Marks, T. J., Efficient carbon-supported heterogeneous molybdenum-dioxo catalyst for chemoselective reductive carbonyl coupling. *Catal. Sci. Technol.* **2017,** *7* (11), 2165-2169.

25. Li, J.; Liu, S.; Lohr, T. L.; Marks, T. J., Efficient Chemoselective Reduction of N-Oxides and Sulfoxides Using a Carbon-Supported Molybdenum-Dioxo Catalyst and Alcohol. *ChemCatChem* **2019,** *11* (16), 4139-4146.

26. Kratish, Y.; Li, J.; Liu, S.; Gao, Y.; Marks, T. J., Polyethylene Terephthalate Deconstruction Catalyzed by a Carbon-Supported Single-Site Molybdenum-Dioxo Complex. *Angewandte Chemie International Edition* **2020,** *59* (45), 19857-19861.

27. Schaetz, A.; Zeltner, M.; Stark, W. J., Carbon Modifications and Surfaces for Catalytic Organic Transformations. *ACS Catalysis* **2012,** *2* (6), 1267-1284.

28. CHAPTER 2 Classification, Structure and Bulk Properties of Nanostructured Carbon Materials. In *Nanostructured Carbon Materials for Catalysis*, The Royal Society of Chemistry: 2015; pp 46-66.

29. Iwanow, M.; Gärtner, T.; Sieber, V.; König, B., Activated carbon as catalyst support: precursors, preparation, modification and characterization. *Beilstein Journal of Organic Chemistry* **2020,** *16*, 1188-1202.

30. Kratish, Y.; Nakamuro, T.; Liu, Y.; Li, J.; Tomotsuka, I.; Harano, K.; Nakamura, E.; Marks, T. J., Synthesis and Characterization of a Well-Defined Carbon Nanohorn-Supported Molybdenum Dioxo Catalyst by SMART-EM Imaging. Surface Structure at the Atomic Level. *Bulletin of the Chemical Society of Japan* **2020,** *94* (2), 427-432.

31. Sarkar, R.; Gupta, A.; Jamatia, R.; Pal, A. K., Reduced graphene oxide supported copper oxide nanocomposites: An efficient heterogeneous and reusable catalyst for the synthesis of ynones, 1,3-diynes and 1,5-benzodiazepines in one-pot under sustainable reaction conditions. *Appl. Organomet. Chem.* **2020,** *34*, e5646.

32. Masteri-Farahani, M.; Mirshekar, S., Covalent functionalization of graphene oxide with molybdenum-carboxylate complexes: New reusable catalysts for the epoxidation of olefins. *Colloids and Surfaces A: Physicochemical and Engineering Aspects* **2018,** *538*, 387-392.

33. Hontoria-Lucas, C.; López-Peinado, A. J.; López-González, J. d. D.; Rojas-Cervantes, M. L.; Martín-Aranda, R. M., Study of oxygen-containing groups in a series of graphite oxides: Physical and chemical characterization. *Carbon* **1995,** *33* (11), 1585-1592.

34. Rattana; Chaiyakun, S.; Witit-anun, N.; Nuntawong, N.; Chindaudom, P.; Oaew, S.; Kedkeaw, C.; Limsuwan, P., Preparation and characterization of graphene oxide nanosheets. *Procedia Engineering* **2012,** *32*, 759-764.

35. Dutta, S.; Bohre, A.; Zheng, W.; Jenness, G. R.; Núñez, M.; Saha, B.; Vlachos, D. G., Solventless C–C Coupling of Low Carbon Furanics to High Carbon Fuel Precursors Using an Improved Graphene Oxide Carbocatalyst. *ACS Catalysis* **2017,** *7* (6), 3905-3915.

36. Dreisch, K.; Andersson, C.; Stahandske, C., Synthesis of MO2Cl2(N,N,N',N'-tetramethylethylenediamine) (M = Mo and W) and crystal structure of WO2Cl2(N,N,N',N'-tetramethylethylenediamine) —an unprecedented coordination geometry in the WO2Cl2 Core. *Polyhedron* **1992,** *11* (17), 2143-2150.

37. Kamenar, B.; Penavić, M.; Korpar-Čolig, B.; Marković, B., Preparation and crystal structure of two oxo-molybdenum complexes with dimethoxyethane. *Inorganica Chim. Acta* **1982,** *65*, L245-L247.

38. Goeta, A. E.; Howard, J. A. K., Low temperature single crystal X-ray diffraction: advantages, instrumentation and applications. *Chemical Society Reviews* **2004,** *33* (8), 490-500.

39. Kim, H.; Kosuda, K. M.; Van Duyne, R. P.; Stair, P. C., Resonance Raman and surface- and tip-enhanced Raman spectroscopy methods to study solid catalysts and heterogeneous catalytic reactions. *Chemical Society Reviews* **2010,** *39* (12), 4820-4844.

40. Dreisch, K.; Andersson, C.; Håkansson, M.; Jangner, S., Diglyme (C6H14O3) complexes of molybdenum and tungsten: crystal structures of [MO2Cl2(C6H14O3)](M = Mo or W). *J. Chem. Soc., Dalton Trans.* **1993,** (7), 1045-1049.

41. Kovtyukhova, N. I.; Ollivier, P. J.; Martin, B. R.; Mallouk, T. E.; Chizhik, S. A.; Buzaneva, E. V.; Gorchinskiy, A. D., Layer-by-Layer Assembly of Ultrathin Composite Films from Micron-Sized Graphite Oxide Sheets and Polycations. *Chem. Mater.* **1999,** *11* (3), 771-778.

42. Kim, F.; Luo, J.; Cruz-Silva, R.; Cote, L. J.; Sohn, K.; Huang, J., Self-Propagating Domino-like Reactions in Oxidized Graphite. *Adv. Funct. Mater.* **2010,** *20* (17), 2867-2873.

43. Ganguly, A.; Sharma, S.; Papakonstantinou, P.; Hamilton, J., Probing the Thermal Deoxygenation of Graphene Oxide Using High-Resolution In Situ X-ray-Based Spectroscopies. *The Journal of Physical Chemistry C* **2011,** *115* (34), 17009-17019.

44. Pavoski, G.; Maraschin, T.; Milani, M. A.; Azambuja, D. S.; Quijada, R.; Moura, C. S.; de Sousa Basso, N.; Galland, G. B., Polyethylene/reduced graphite oxide nanocomposites with improved morphology and conductivity. *Polymer* **2015,** *81*, 79-86.

45. Luo, J.; Cote, L. J.; Tung, V. C.; Tan, A. T. L.; Goins, P. E.; Wu, J.; Huang, J., Graphene Oxide Nanocolloids. *Journal of the American Chemical Society* **2010,** *132* (50), 17667-17669.

46. Xu, B.; Yue, S.; Sui, Z.; Zhang, X.; Hou, S.; Cao, G.; Yang, Y., What is the choice for supercapacitors: graphene or graphene oxide? *Energy Environ. Sci.* **2011,** *4* (8), 2826-2830.

47. Krishnamoorthy, K.; Veerapandian, M.; Mohan, R.; Kim, S.-J., Investigation of Raman and photoluminescence studies of reduced graphene oxide sheets. *Applied Physics A* **2012,** *106* (3), 501-506.

48. Stobinski, L.; Lesiak, B.; Malolepszy, A.; Mazurkiewicz, M.; Mierzwa, B.; Zemek, J.; Jiricek, P.; Bieloshapka, I., Graphene oxide and reduced graphene oxide studied by the XRD, TEM and electron spectroscopy methods. *J. Electron Spectros. Relat. Phenomena* **2014,** *195*, 145-154.

49. Bian, G.; Jiang, P.; Zhang, W.; Jiang, K.; Hu, L.; Jian, Z.; Shen, Y.; Zhang, P., A novel poly(p-styrenesulfonic acid) grafted carbon nanotube/graphene oxide architecture with enhanced catalytic performance for the synthesis of benzoate esters and fatty acid alkyl esters. *RSC Adv.* **2015,** *5* (110), 90757-90765.

50. Cheng, Y.; Zhao, Q.; Li, Y.; Peng, W.; Zhang, G.; Zhang, F.; Fan, X., Gold nanoparticles supported on layered TiO2–RGO hybrid as an enhanced and recyclable catalyst for microwave-assisted hydration reaction. *RSC Advances* **2016,** *6* (80), 76151-76157.

51. Spevack, P. A.; McIntyre, N. S., Thermal reduction of molybdenum trioxide. *J. Phys. Chem.* **1992,** *96* (22), 9029-9035.

52. Luekittisup, P.; Tanboonchauy, V.; Chumee, J.; Predapitakkun, S.; Kiatkomol, R. W.; Grisdanurak, N., Removal of Chlorinated Chemicals in H₂ Feedstock Using Modified Activated Carbon. *Journal of Chemistry* **2015,** *2015*, 959012.

53. Tsubouchi, N.; Mochizuki, Y.; Shinohara, Y.; Kawashima, A.; Ohtsuka, Y., Low-Temperature Reactions of HCl with Metal-Doped Carbon. *Energy & Fuels* **2018,** *32* (6), 6970-6977.

54. Xie, S.; Chen, K.; Bell, A. T.; Iglesia, E., Structural Characterization of Molybdenum Oxide Supported on Zirconia. *The Journal of Physical Chemistry B* **2000,** *104* (43), 10059-10068.

55. Mercera, P. D. L.; van Ommen, J. G.; Doesburg, E. B. M.; Burggraaf, A. J.; Ross, J. R. H., Zirconia as a support for catalysts Influence of additives on the thermal stability of the porous texture of monoclinic zirconia. *Applied Catalysis* **1991,** *71* (2), 363-391.

56. Panda, D.; Nandi, A.; Datta, S. K.; Saha, H.; Majumdar, S., Selective detection of carbon monoxide (CO) gas by reduced graphene oxide (rGO) at room temperature. *RSC Advances* **2016,** *6* (53), 47337-47348.

57. Extrand, C. W., Uncertainty in contact angle measurements from the tangent method. *Journal of Adhesion Science and Technology* **2016,** *30* (15), 1597-1601.

58. Akbarpour, S.; Bezaatpour, A.; Askarizadeh, E.; Amiri, M., Covalent supporting of novel dioxo-molybdenum tetradentate pyrrole-imine complex on Fe3O4 as high-efficiency nanocatalyst for selective epoxidation of olefins. *Appl. Organomet. Chem.* **2017,** *31* (11), e3804.

59. Hanna, T. A.; Ghosh, A. K.; Ibarra, C.; Mendez-Rojas, M. A.; Rheingold, A. L.; Watson, W. H., Steric Control of Coordination Number: A Series of Mo(VI) Dioxo Diaryloxide Complexes Bearing 4-, 5-, and 6-Coordinate Environments. *Inorganic Chemistry* **2004,** *43* (4), 1511-1516.

60. Dai, H.; Gong, L.; Zhang, S.; Xu, G.; Li, Y.; Hong, Z.; Lin, Y., All-in-one bioprobe devised with hierarchical-ordered magnetic NiCo2O4 superstructure for ultrasensitive dual-readout

immunosensor for logic diagnosis of tumor marker. *Biosens. Bioelectron.* **2016,** *77*, 928-935.

61. Santos, B. M.; Zhao, W.; Zotin, J. L.; Silva, M. A. P. d.; Oliviero, L.; Maugé, F., Impact of proximity between NiMoS and zeolitic HY sites on cyclohexene hydroconversion: An infrared operando study of sulfide catalysts. *Journal of Catalysis* **2021,** *396*, 92-103.

62. Rodriguez, J.; Conley, M. P., Ethylene Polymerization Activity of (R3P)Ni(codH)+ (cod = 1,5-cylcooctadiene) Sites Supported on Sulfated Zirconium Oxide. *Inorganic Chemistry* **2021,** *60* (10), 6946-6949.

63. Yang, Q.; Xu, W.; Gong, S.; Zheng, G.; Tian, Z.; Wen, Y.; Peng, L.; Zhang, L.; Lu, Z.; Chen, L., Atomically dispersed Lewis acid sites boost 2-electron oxygen reduction activity of carbon-based catalysts. *Nature Communications* **2020,** *11* (1), 5478.

64. Mizuno, K.; Ikeda, M.; Imokawa, T.; Take, J.-i.; Yoneda, Y., Nature of Catalytically Active Sites over Solid Acids. I. Selective Poisoning of Lewis Acid Sites on Silica–Alumina with Pyridine and Its Application to Olefin Polymerization. *Bulletin of the Chemical Society of Japan* **1976,** *49* (7), 1788-1793.

65. Amakawa, K.; Wrabetz, S.; Kröhnert, J.; Tzolova-Müller, G.; Schlögl, R.; Trunschke, A., In Situ Generation of Active Sites in Olefin Metathesis. *Journal of the American Chemical Society* **2012,** *134* (28), 11462-11473.

66. Lwin, S.; Wachs, I. E., Olefin Metathesis by Supported Metal Oxide Catalysts. *ACS Catalysis* **2014,** *4* (8), 2505-2520.

67. Zhuo, H.-Y.; Zhang, X.; Liang, J.-X.; Yu, Q.; Xiao, H.; Li, J., Theoretical Understandings of Graphene-based Metal Single-Atom Catalysts: Stability and Catalytic Performance. *Chemical Reviews* **2020,** *120* (21), 12315-12341.
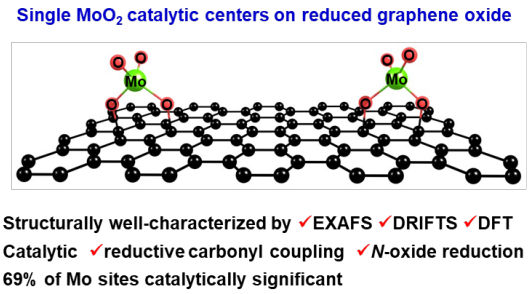
TOC GRAPHIC